

State-space modeling of intra-seasonal persistence in daily climate indices: a data-driven approach for seasonal forecasting

Philip G. Sansom, David B. Stephenson and Daniel B. Williamson
University of Exeter, Exeter, United Kingdom

Abstract

Existing methods for diagnosing predictability in climate indices often make a number of unjustified assumptions about the climate system that can lead to misleading conclusions. We present a flexible family of state-space models capable of separating the effects of external forcing on inter-annual time scales, from long-term trends and decadal variability, short term weather noise, observational errors and changes in autocorrelation. Standard potential predictability models only estimate the fraction of the total variance in the index attributable to external forcing. In addition, our methodology allows us to partition individual seasonal means into forced, slow, fast and error components. Changes in the predictable signal within the season can also be estimated. The model can also be used in forecast mode to assess both intra- and inter-seasonal predictability.

We apply the proposed methodology to a North Atlantic Oscillation index for the years 1948–2017. Around 60% of the inter-annual variance in the December-January-February mean North Atlantic Oscillation is attributable to external forcing, and 8% to trends on longer time-scales. In some years, the external forcing remains relatively constant throughout the winter season, in others it changes during the season. Skillful statistical forecasts of the December-January-February mean North Atlantic Oscillation are possible from the end of November onward and predictability extends into March. Statistical forecasts of the December-January-February mean achieve a correlation with the observations of 0.48.

1 Introduction

Many processes in the climate system are only active or only interact intermittently. Snow cover changes the interaction between the land surface and the atmosphere [e.g., Chapin III et al., 2010]. Sea ice alters the coupling between the ocean and the atmosphere [e.g., Bourassa et al., 2013]. Stratosphere-troposphere coupling are known to influence storm tracks and surface weather [e.g., Kidston et al., 2015]. El Niño and La Niña events influence weather patterns in remote regions [e.g., Toniazzo and Scaife, 2006]. Intermittent forcing is often associated with unusually persistent weather conditions [Brönnimann, 2007, Tomassini et al., 2012]. Therefore, such events are a potential source of skill for short-term climate forecasts [Sigmond et al., 2013, Scaife et al., 2014].

The concept of potential predictability in climate indices was introduced by [Madden, 1976] and formalized by Zwiers [1987] using analysis of variance methods. The observed variance in the climate index is partitioned into inter-annual and intra-seasonal components. Observations within seasons are used to estimate the inter-annual variance in the seasonal mean index that might be expected due to unforced natural variability, i.e., weather. This estimate is compared with the observed inter-annual variance of the seasonal mean index to determine if some part of the observed process might be attributed to external forcing and be “potentially predictable”.

Existing methods for assessing potential predictability have two main limitations. First, the climate is assumed to be stationary (constant mean and variance) throughout the study

period. Fixed trends and seasonal cycles are often estimated and removed from the data. Gradual changes in the mean or seasonal cycle due to natural or anthropogenic forcing can be confounded with potentially predictable signals on seasonal time-scales, artificially inflating the signal or making it hard to detect. Second, data are often split into arbitrarily defined seasons and analyzed separately. Analyzing seasons separately leads to a loss of information by ignoring components common to all seasons. Conversely, if a predictable signal only exists for part of a season, then it may be difficult to detect over whole season. In addition, separate autocorrelation functions are often estimated for each season. This makes it difficult to distinguish changes in the inter-annual variance of the seasonal mean, from changes in the autocorrelation structure.

Sansom et al. [2018] proposed a more flexible state-space time series approach to assessing potential predictability that directly addresses the limitations of existing methods. The new methodology allows a whole time series to be analyzed without being split into seasons. The timing of the external forcing can be inferred from the data. Predictable behavior due to temporary changes in the mean can be distinguished from behavior due to temporary changes in the autocorrelation structure. Non-stationary mean, trend and seasonal components are estimated simultaneously to avoid confounding other potentially predictable signals. Gradual changes in the autocorrelation structure can also be estimated.

In addition to estimating the fraction of inter-annual variance explained by external forcing, the new methodology allows us to address a number of more detailed questions. For example, was a particular extreme season the result of external forcing, or simply natural variability? To answer this, individual seasonal means can be decomposed into mean, weather, error and externally forced components. Using the new methodology, the external forcing effect can vary continuously, rather than being fixed throughout a season. Therefore, we can examine changes in the forcing within seasons, and persistence between seasons. The new statistical model can also be used to forecast climate indices, either by rapidly learning the state of the external forcing within a season, or by exploiting inter-annual persistence in the forced component.

Sansom et al. [2018] demonstrated their methodology on a short time series of a daily North Atlantic Oscillation (NAO) index and used a complex and expensive Markov Chain Monte Carlo (MCMC) procedure to estimate key parameters. In this study, we develop a simplified maximum likelihood approach to parameter estimation that is more efficient and can be easily implemented without specialist statistical knowledge. We analyze a longer 70-year daily NAO index computed from a different data source and compare the results to previous potential predictability studies. Results are presented for all seasons, rather than just boreal winter and summer. The longer time series allows us to investigate multi-decadal trends in the NAO and time-varying skill in seasonal forecasts. We also compare the skill of seasonal forecasts from the statistical model with that of the state-of-the-art GloSea5 seasonal forecasting system [MacLachlan et al., 2015]. Our code is freely available to enable our results to be reproduced, and our methodology to be easily applied to other climate indices.

The remainder of this study is structured as follows, Section 2 describes the construction and features of the NAO index. In Section 3 we summarize the statistical model proposed by Sansom et al. [2018] for diagnosing persistence and predictability. Section 4 outlines the process of model building, parameter estimation by maximum likelihood, and model checking. In Section 5 we present the results of our analysis of the the 70-year NAO index. Section 6 concludes with a discussion.

2 Data

In this study, we analyze a daily NAO index computed from the NCEP/NCAR reanalysis [Kalnay et al., 1996]. Following Stephenson et al. [2006], the NAO index is calculated as the difference in area averaged mean sea level pressure between two rectangular regions stretching from 20° – 55° N and 55° – 90° N, both spanning 90° W– 60° E. This definition provides a consistent daily index for the whole year that is robust to seasonal changes in the centers of action of the NAO. By using a single definition of the NAO throughout the year we avoid possible

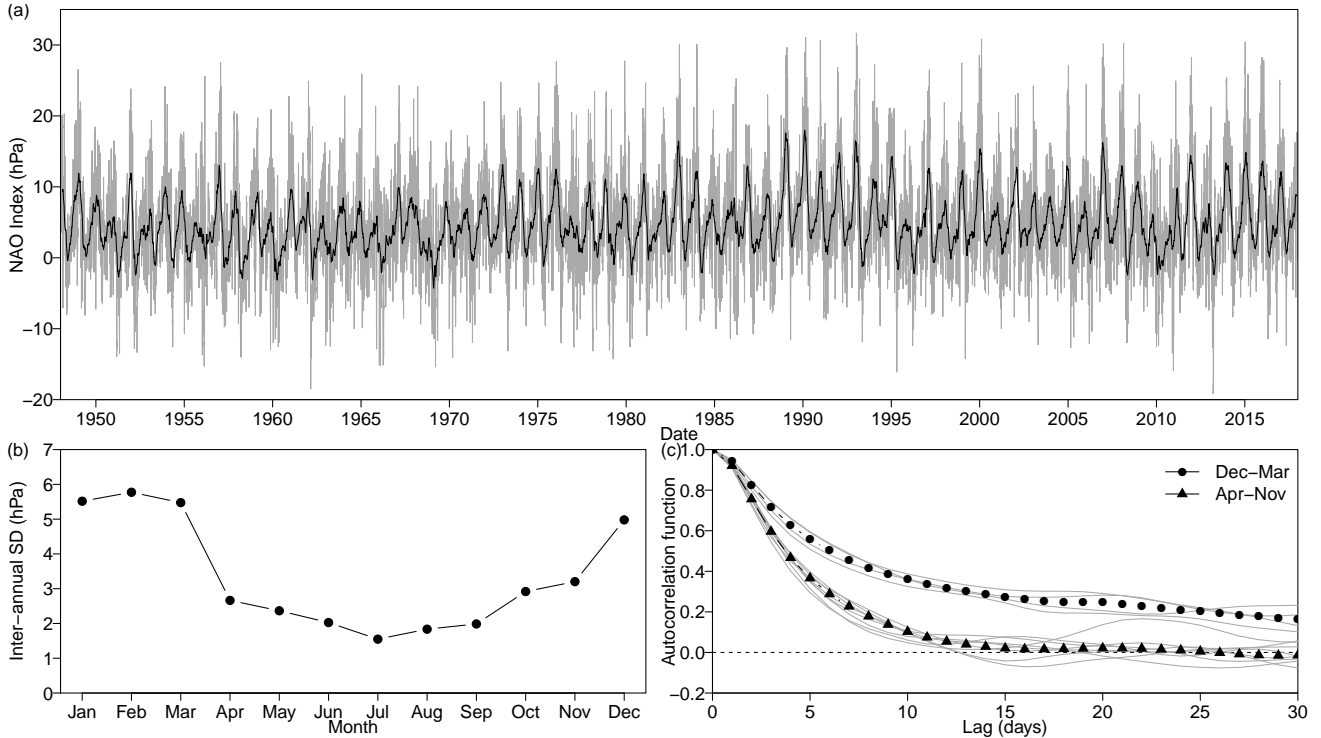


Figure 1: The North Atlantic Oscillation index. (a) Daily time series (grey) and 90 day moving average (black) of our NAO index, (b) the inter-annual standard deviation of the monthly mean NAO index, and (c) the autocorrelation function of the daily NAO index computed for each month of the year.

inconsistencies where multiple definitions are joined together. Working directly with a pressure index rather than a principle component index improves the interpretability of the model. By working in the natural units of pressure, we can more easily incorporate quantitative judgments about model components and assess whether our inferences are intuitively reasonable.

The daily NAO index computed from the NCEP/NCAR reanalysis is shown in Figure 1(a) and spans the period 1 January 1948 to 31 December 2017, a total of 25,568 daily values. An annual cycle is clearly visible. Figure 1(a) shows the inter-annual variance of the monthly mean NAO index. The inter-annual variance during December–March is between two and three times higher than during April–November. Figure 1(b) shows the autocorrelation function of the daily NAO index for each month of the year, after detrending and deseasonalizing the data. The autocorrelation in the NAO index is also stronger during December–March than during April–November. Figures 1(b) and (c) suggest a persistent change in the dynamics of the daily NAO index during December–March.

3 Methodology

3.1 Potential predictability

The concept of potential predictability for climate indices was formalized by Zwiers [1987] (see also Chapter 17.2 of von Storch and Zwiers [1999]). One of the simplest formulations of the basic statistical model for potential predictability is

$$\begin{aligned}
 Y_{i,j} &= Z_j + X_{i,j} & Z_j &\sim N(0, \sigma_Z^2) \\
 X_{i,j} &= \phi X_{i-1,j} + w_{i,j} & w_{i,j} &\sim N(0, \sigma_w^2)
 \end{aligned}$$

where Y is the observed climate index and the index i denotes the time within a season and j denotes the year. The time series $X_{i,j}$ represents noise due to weather and is modeled as an autoregressive process with coefficient ϕ ($-1 < \phi < 1$), forced by a normal random walk (Gaussian white noise) $w_{i,j}$. The quantity Z_j represents the externally forced signal and is assumed independent and identically distributed between years j . The underlying assumption is that Z_j varies slowly (i.e., predictably) and can be assumed constant within a particular season, while $X_{i,j}$ varies rapidly throughout the season. The total variance in Y_j is partitioned into inter-annual variance due to Z_j and intra-seasonal variance due to weather $X_{i,j}$.

The basic potential predictability model above implicitly assumes that the long-term mean of the observed process Y is zero. If this is not the case, then the mean must first be estimated and removed. In order to estimate potential predictability in different seasons, the model must be fitted to each season separately. Fitting each season separately makes it difficult to distinguish changes in the variance of the seasonal mean σ_Z^2 from changes in the day-to-day persistence ϕ .

3.2 A more flexible approach

Sansom et al. [2018] proposed a more flexible statistical model for diagnosing persistence and predictability in time series, which we summarize here. A climate index Y_t ($t = 1, \dots, T$) is modeled as the sum of mean, seasonal, weather and intermittently forced components

Forecast equation

$$Y_t = \mu_t + \sum_{k=1}^K \psi_{kt} + X_t + Z_t + v_t \quad v_t \sim N(0, V)$$

Mean component

$$\begin{aligned} \mu_t &= \mu_{t-1} + \beta_t + w_{\mu t} & w_{\mu t} &\sim N(0, W_\mu) \\ \beta_t &= \beta_{t-1} + w_{\beta t} & w_{\beta t} &\sim N(0, W_\beta) \end{aligned}$$

Seasonal component

$$\begin{aligned} \psi_{kt} &= \psi_{k,t-1} \cos k\omega + \psi_{k,t-1}^* \sin k\omega + w_{\psi_{kt}} & w_{\psi_{kt}} &\sim N(0, W_\psi) \\ \psi_{kt}^* &= \psi_{k,t-1}^* \cos k\omega - \psi_{k,t-1} \sin k\omega + w_{\psi_{kt}^*} & w_{\psi_{kt}^*} &\sim N(0, W_\psi) \end{aligned}$$

Weather component

$$\begin{aligned} X_t &= \sum_{p=1}^P \phi_{pt} X_{t-p} + w_{Xt} & w_{Xt} &\sim N(0, W_{Xt}) \\ \phi_{pt} &= \phi_{p,t-1} + w_{\phi_{pt}} & w_{\phi_{pt}} &\sim N(0, W_\phi) \end{aligned}$$

for $k = 1, \dots, K$ and $p = 1, \dots, P$ where $\omega = 2\pi/365.25$. The residual v_t represents observation or measurement error. The expected size of the errors is controlled by the variance V . The parameters μ_t and β_t represent the mean and trend respectively. The harmonic parameters ψ_{kt} and ψ_{kt}^* ($k = 1, \dots, K$) represent seasonal or other cyclic behavior. Gradual changes in the mean, trend and seasonal parameters are captured by the normal random walks $w_{\mu t}$, $w_{\beta t}$, $w_{\psi_{kt}}$ and $w_{\psi_{kt}^*}$. The variances W_μ , W_β and W_ψ control the rate of change of each component. The weather component X_t represents the day-to-day variability in the NAO index and is modeled as a *time-varying* autoregressive process [Prado and West, 2010]. Gradual changes in the daily autocorrelation structure are captured by normal random walks $w_{\phi_{pt}}$ on the autoregressive coefficients $\phi_{1t}, \dots, \phi_{Pt}$. The variance W_ϕ controls the rate of change of the autoregressive coefficients. For many climate indices, including the NAO, the day-to-day variance W_{Xt} of the weather component X_t will vary with the annual cycle and can be modeled as

$$W_{Xt} = W_X + \sqrt{a^2 + b^2} + a \sin \omega t + b \cos \omega t \quad W_X > 0.$$

The intermittently forced component

We consider two alternative models for the effect of intermittent forcing leading to unusual persistence – a temporary change in the mean, or a temporary change in the day-to-day persistence of the weather conditions. Figure 1 suggests a change in the persistence of the NAO

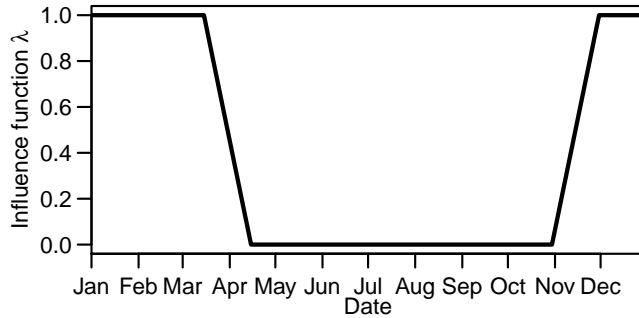


Figure 2: The influence function λ_t chosen for the NAO index. The intermittent forcing only affects the observed index when $\lambda_t > 0$.

between December and March. We represent the timing of the timing of the forcing effect using an indicator variable

$$\lambda_t = \begin{cases} 0 & \text{in Apr–Nov} \\ 1 & \text{in Dec–Mar.} \end{cases}$$

In practice, we allow a brief transition period between the two regimes by interpolating between 0 and 1 over a short time. We will refer to λ_t as the influence function and the period when $\lambda > 0$ as the forcing period. Figure 2 shows the influence function chosen for the NAO index in Section 4

A temporary shift in the mean can be captured by introducing a new variable δ_t and writing the intermittently forced component as

$$Z_t = \lambda_t \delta_t$$

where the shift δ_t is modeled as

$$\delta_t = \varphi \delta_{t-1} + w_{\delta t} \quad w_{\delta t} \sim N(0, W_\delta).$$

The mean shift δ_t is analogous to the seasonal mean Z_j in the basic potential predictability model, but varies continuously rather than being assumed constant throughout a season and independent between years. The shift only affects the observed process Y_t when $\lambda_t > 0$. Depending on the values of φ ($-1 < \varphi < 1$) and W_δ ($W_\delta > 0$) the mean shift δ_t can persist between winters ($\varphi \approx 1$, $W_\delta \approx 0$) or vary during a single season ($\varphi < 1$, $W_\delta > 0$).

A temporary change in the day-to-day persistence can be represented by writing the intermittently forced component as

$$Z_t = \lambda_t \sum_{p=1}^P \delta_{pt} X_{t-p}.$$

where the P new variables δ_{pt} alter the autocorrelation structure of the weather component X_t and are modeled as

$$\delta_{pt} = \varphi \delta_{p,t-1} + w_{\delta_{pt}} \quad w_{\delta_{pt}} \sim N(0, W_\delta).$$

If the winter behavior in Figure 1 is caused by a change in the persistence of day-to-day weather conditions, then we might expect the change to be similar each year, i.e., $\varphi \approx 1$ and $W_\delta \approx 0$.

3.3 Model fitting

Sansom et al. [2018] developed efficient model fitting procedures based on the Extended Kalman Filter [Durbin and Koopman, 2012, Chapter 10]. Model outputs take the form of plausible trajectories for the time evolution of each component $\mu_t, \beta_t, \psi_{1t}, \psi_{1t}^*, \dots, \psi_{Kt}, \psi_{Kt}^*, X_t, \phi_{1t}, \dots, \phi_{Pt}$

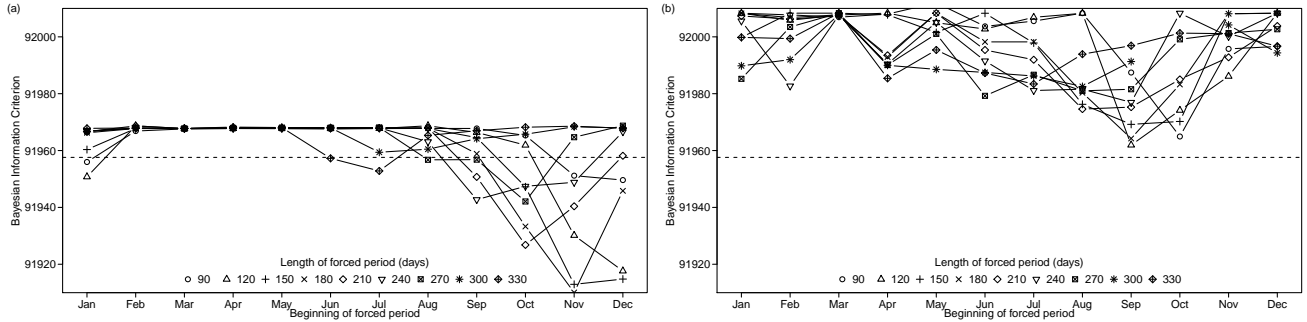


Figure 3: Choice of influence function λ_t . Bayesian Information Criterion (lower is better) of models with forced periods from 3–11 months starting on the first day of each month were considered. The dashed line indicates the model with no predictable signal. The influence function was linearly tapered during the first and last 30 days of the forced period, as in Figure 2.

and δ_t . Both point and interval estimates can be constructed from samples of plausible trajectories for any combination of parameters or time points of interest. Forecasting from the fitted model can be achieved simply by simulating from the equations in the previous section. See Sansom et al. [2018] for full details.

4 Modeling the North Atlantic Oscillation index

In order to fit the model described in the previous section to our NAO index, we need to specify the following quantities:

- the number of harmonic components K ;
- the order of the autoregressive process P ;
- the variances V , W_μ , W_β , W_ψ , W_{X_t} and W_ϕ ;
- the forcing parameters φ and W_δ ;
- the influence function λ_t ;
- initial guesses for μ_t , β_t , ψ_{1t} , ψ_{1t}^* , \dots , ψ_{Kt} , ψ_{Kt}^* , X_t , \dots , X_{t-P+1} , ϕ_{1t} , \dots , ϕ_{Pt} and δ_t at time $t = 0$.

Exploratory analysis of the daily NAO index suggests a model with annual and semi-annual cycles ($K = 2$) for the seasonal component, and a fifth order autoregressive model ($P = 5$) for the weather component (see supplementary material for details). Our initial guesses for the state parameters and the maximum likelihood estimates of the variance parameters are also given in the supplementary material.

We estimate the V , W_μ , W_β , W_ψ , W_ϕ and W_{X_t} and the forcing parameters φ and W_δ by maximum likelihood, using the expression for the likelihood provided in Sansom et al. [2018]. To ensure the variances estimates were positive, we estimated the log of each parameter. We recommend using a quasi-Newton method such as the Broyden-Fletcher-Goldfarb-Shanno algorithm for numerical maximization of the likelihood. Simplex methods such as Nelder-Mead optimization will tend to be unstable if any of the variances are very close to zero.

Mean shift or autocorrelation shift?

Figure 1 suggests the presence of external forcing of the NAO between December and March. In order to discover any other external forcing, a family of 108 different influence functions λ_t was constructed. We considered forced periods starting on the first day of each month, with lengths between 90 and 330 days in 30 day increments, linearly tapered over the first and last 30 days,

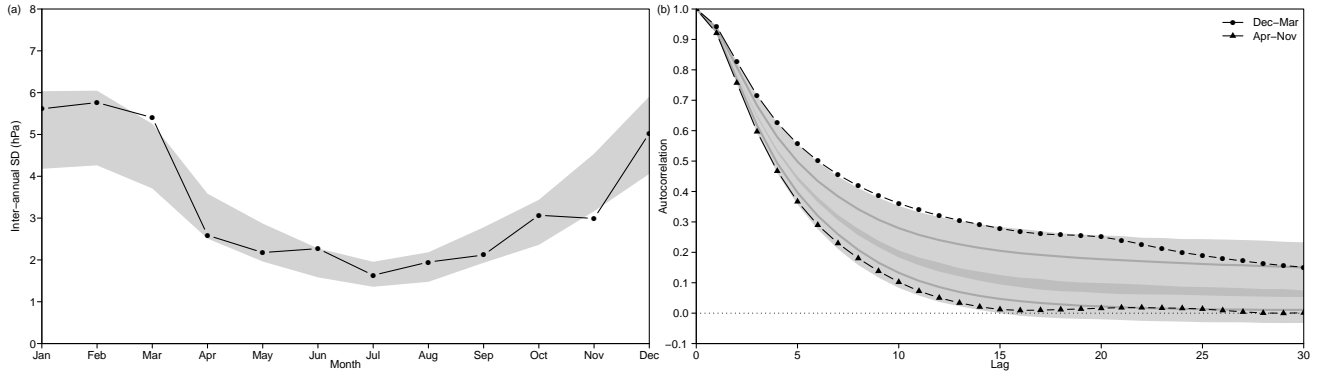


Figure 4: Posterior predictive checks. (a) The inter-annual standard deviation of the monthly mean NAO index, and (b) the autocorrelation function of the daily NAO index computed for Dec-Mar and Apr-Nov. Black lines represent the sample estimates computed from the observed NAO index as in Figure 1. Shaded grey regions represent 95% credible intervals computed from 1000 simulations of the 50 years between 1968 and 2017 from the statistical model.

as in Figure 2. Maximum likelihood estimation of the variance and forcing parameters was carried out for each influence function, for both the mean shift model, and the autocorrelation shift model.

Figure 3 compares the two families of models using the Bayesian Information Criteria [Wilks, 2011, Chapter 9]. In the mean shift model, there is no evidence of potentially predictable periods beginning between February and July. The best models have potentially predictable periods that begin in November or December, and end in March or April. In comparison, the autocorrelation shift model performs very poorly. There is little discrimination between the different influence functions, and none outperform a model with no external forcing. This agrees with the conclusions of Sansom et al. [2018] who analyzed a shorter NAO index but considered a much larger family of influence functions by Markov Chain Monte Carlo simulation. We conclude that a temporary mean shift is the most likely explanation for the persistent behavior of the winter NAO, and do not consider the autocorrelation model further.

Model checking

We used simulations of the NAO index between 1968 and 2017 to check whether the mean shift model can adequately reproduce the behavior observed in Figure 1. The model with $P = 5$ struggled to reproduce the summer autocorrelation function (see supplementary material). We settled on a model with $P = 6$ and a 165 day forced period beginning on 1 Nov each year. The influence function λ_t is shown in Figure 2.

Figure 4 shows that the chosen model is able to reproduce the observed patterns of both the inter-annual variance and the autocorrelation function. The pronounced step in the inter-annual variance between December and March is captured reasonably well. There is also a clear difference between the autocorrelation functions simulated for Dec-Mar and Apr-Nov, although parts of the observed autocorrelation in Dec-Mar lie on the very edge of the simulated 95% credible interval. We conclude that a mean shift model is able to explain the observed features of the NAO index. Simulation studies from the optimal autocorrelation shift model are included in the supplementary material for comparison, however it was unable to reproduce the observed inter-annual variance or autocorrelation function.

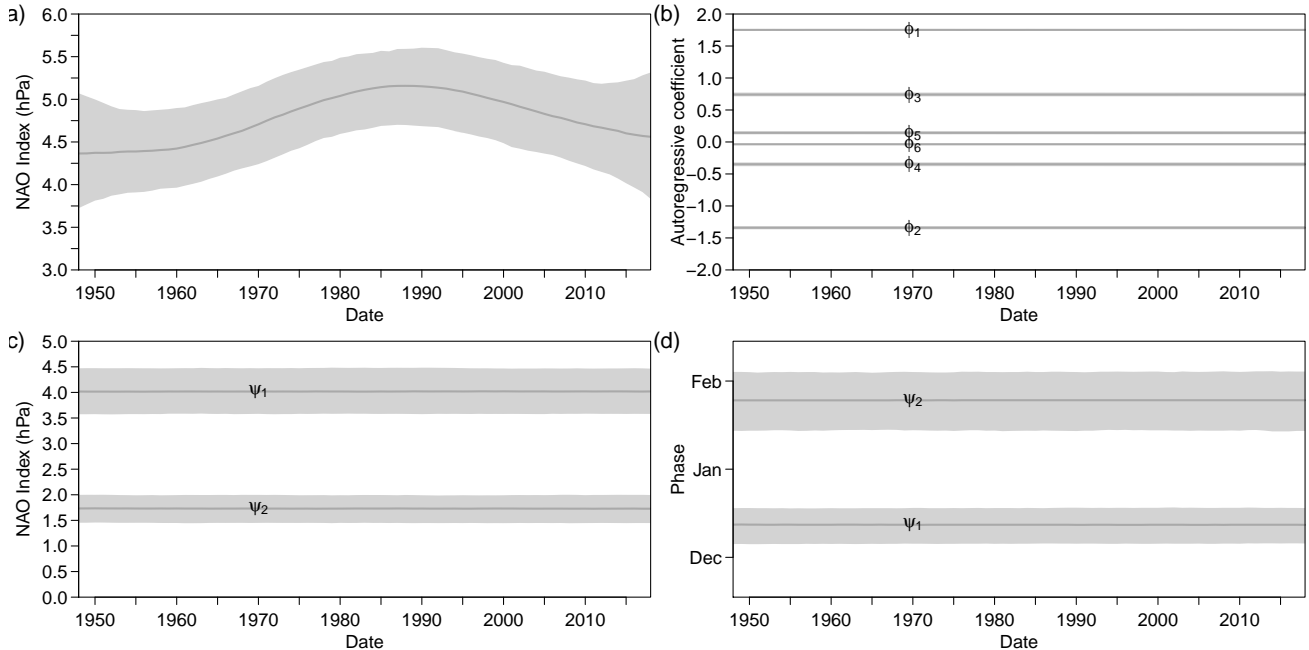


Figure 5: Long-term trends. (a) The long-term mean component μ_t , (b) the autoregressive coefficients $\phi_{1t}, \dots, \phi_{6t}$, (c) the amplitude of the annual and semi-annual cycles ψ_{1t} and ψ_{2t} , (d) the phase of the annual and semi-annual cycles ψ_{1t} and ψ_{2t} plotted as the timing the first peak. Solid lines indicate the posterior mean and shading represents 95 % credible intervals computed from 1000 plausible trajectories for the state parameters $\theta_1, \dots, \theta_T$.

5 Results

5.1 Long-term behavior of the NAO index

The mean component μ_t is intended to capture gradual changes due to climate change or long-term decadal variability. Figure 5(a) suggests that the mean of the NAO index has changed gradually over the last 70 years. The mean μ_t rose by around 0.8 hPa (95% C.I. 0.1 hPa–1.3 hPa) between 1950 and 1990, before declining slightly over the following two decades. In contrast, the amplitude and phase of the annual and semi-annual cycles in Figures 5(c) and (d) show little sign of variation. Figure 5(b) also shows very little change in the autoregressive coefficients ϕ_1, \dots, ϕ_6 over the study period. This suggests that the seasonal behavior and autocorrelation of the daily NAO index have been effectively constant over the last 70 years, and have not contributed to periods of unusual persistence.

5.2 Analysis of variance

Sansom et al. [2018] describe how standard analysis of variance methods can be applied to our model for the daily NAO index. Table 1 lists the fraction of inter-annual variance explained by each component for the traditional climatological seasons. The contribution due to observation error v_t is always negligible. This is due to the fact that our NAO index is computed from reanalysis data. While there will be errors in the underlying observations, there should be no independent errors between time steps in the reanalysis output.

In DJF, the potentially predictable component explains around 60 % (95 % credible interval 48 %–70 %) of the inter-annual variance in the seasonal mean NAO index, compared to 32 % (24 %–40 %) for the weather component. The remaining 8 % (1 %–17 %) is explained by changes in the mean. This implies a potential correlation of almost 0.8 for a perfect forecast, similar to the findings of Scaife et al. [2014] and Athanasiadis et al. [2017]. In JJA there is no external

Table 1: Analysis of variance. Bracketed values indicate 95% credible intervals.

	Mean	External	Weather	Error
MAM	0.05 (0.00,0.11)	0.35 (0.22,0.46)	0.60 (0.49,0.71)	0.00 (0.00,0.00)
JJA	0.13 (0.05,0.16)	0.00 (0.00,0.00)	0.87 (0.84,0.95)	0.00 (0.00,0.00)
SON	0.03 (0.01,0.05)	0.11 (0.04,0.20)	0.86 (0.77,0.93)	0.00 (0.00,0.00)
DJF	0.08 (0.01,0.17)	0.60 (0.48,0.70)	0.32 (0.24,0.40)	0.00 (0.00,0.00)

forcing our final model. Around 87% (84%–95%) of the inter-annual variance is attributed to weather X_t . The remaining 13% (5%–16%) is attributed to slow changes in the mean.

For comparison, we repeated the analysis of Keeley et al. [2009] using the canonical model of Zwiers [1987] on our simple NAO index. Fixed annual and semi-annual harmonics were estimated by least squares and removed from the data before analysis. In DJF, the “best guess” method of Keeley et al. [2009] suggests that around 75% of the inter-annual variance is attributable to external forcing, and 25% to weather noise. These estimates are only just outside of our 95% credible intervals. The difference is partially explained by the contribution due to changes in the mean, which in the method of Keeley et al. [2009] will have been included in the contribution due to external forcing. In JJA, the Keeley et al. [2009] method estimates that around 84% of the inter-annual variance is attributable to weather and 16% to external forcing. It seems that simple potential predictability methods are able to estimate the contribution due to weather noise reasonably accurately, but by definition it cannot distinguish changes in the mean from external forcing.

Using empirical mode decomposition on a related index, Franzke and Woollings [2011] estimated that around 55% of the inter-annual variance in the winter NAO could be explained by external forcing. This is very similar to our estimate of 60%, since empirical mode decomposition also accounts for long-term trends. Franzke and Woollings [2011] also estimated that up to 30% of the inter-annual variance in summer can also be explained by external forcing. By fitting a single forcing effect, we have focused on the extended winter period. Figure 3 suggests that there may also be short period of limited predictability in summer, however further investigation is beyond the scope of this study.

5.3 What happened in particular years?

Figure 6 shows the estimated contributions of the mean μ_t , potentially predictable Z_t , weather X_t , and observation error v_t components of the model to the winter (DJF) mean NAO index during each year of the study period. The slow increase to slight decrease in the long-term mean μ_t of the NAO is clearly visible in the white bars corresponding the mean component μ_t . The contributions of the forced Z_t and weather X_t components appear positively correlated ($\rho = 0.69$), despite being independent in the model. The estimates presented in Fig. 6 are a summary of 1000 plausible trajectories $t = 1, \dots, T$ for each component. The positive correlation is an anomaly caused by summarizing over the sample of plausible trajectories. If the forcing effect δ_t is too weak to distinguish in a particular year, then on average the seasonal mean will be partitioned roughly in line with the analysis of variance in Tab. 1, leading to correlated estimates of the the forced Z_t and weather X_t components. The fact that the relative contributions of the forced and weather components varies significantly, and in some years have different signs (e.g., 1961), indicates that the model is able to distinguish the two effects. If the two components were actually correlated, then we would expect the seasonal means of each component from each individual trajectory to also be correlated. This is not the case, performing the same attribution analysis for each individual trajectory returns an average correlation of $\rho = 0.02$ ($-0.13, +0.21$).

Figure 7 shows the estimated evolution of the forcing effect δ_t during four recent winters with unusually strong winter NAO anomalies. Previous studies assumed that any external forcing was constant throughout a particular season [e.g., Keeley et al., 2009]. Our analysis suggests

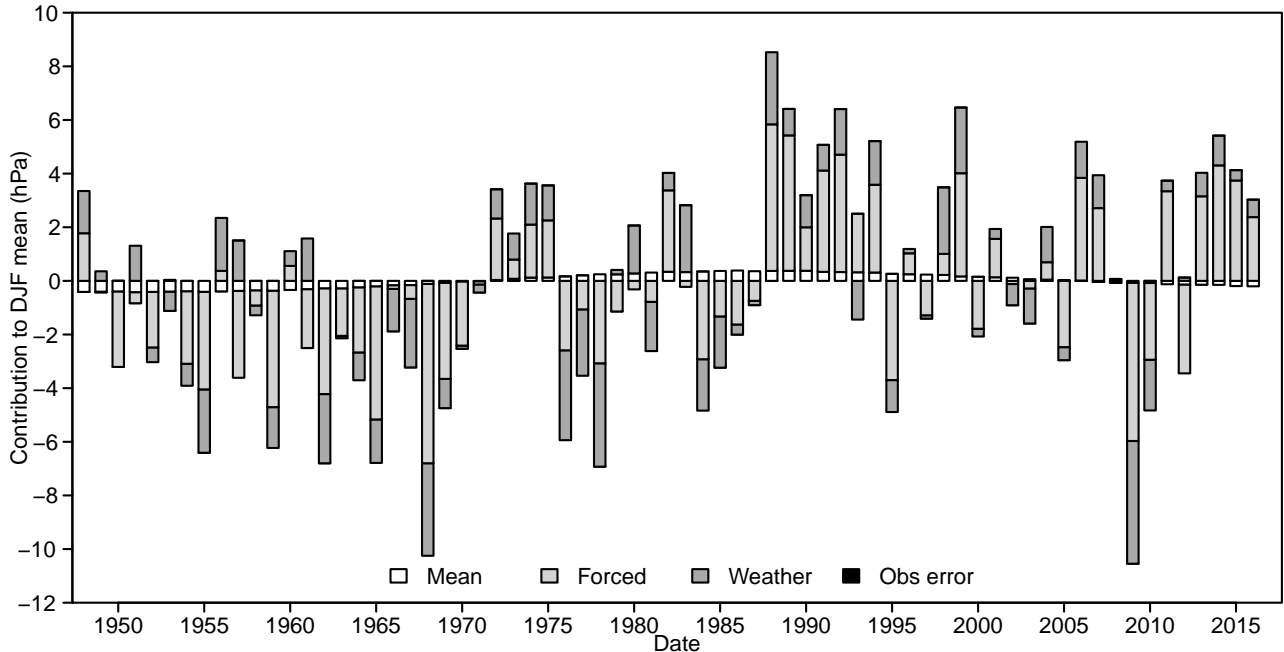


Figure 6: The posterior mean contribution of the mean, potentially predictable, weather and observation error components to the DJF mean NAO index every year between 1958 and 2017, computed from 1000 plausible trajectories for the state parameters.

that the assumption of constant forcing is not justified. In 1989–90, the forcing effect increased in strength throughout December and January, reaching a peak during February. February 1990 was marked by a series of eight strong extra-tropical cyclones impacting Europe. The strong positive NAO in 1989–90 has been linked to a strong La Niña event [e.g., Brönnimann et al., 2006]. In 1992–93 and 1995–96 the forcing effect remained fairly constant throughout the winter season. In 2009–10 the forcing effect started out only moderately negative during November before increasing in strength during December, January and February. The strong negative NAO in 2009–10 has been linked to a strong El Niño event and an associated sudden stratospheric warming [Fereday et al., 2012, Scaife et al., 2016].

5.4 Seasonal predictability

Between December and March, the forcing effect δ_t represents a slowly varying shift in the mean of the NAO index. If we can estimate the external forcing early in the season, then we should have useful predictability for the rest of the winter. Figure 8 shows the results of forecast tests for the seasonal mean NAO index. 1000 forecast members were initialized on the first day of each season (1 March, 1 June, 1 September and 1 December) for every year between 1957 and 2016 and propagated forward until the end of that season. This differs from standard practice in seasonal forecasting where forecasts are usually initialized 30 days before the beginning of the season. However, since the forced period selected in Section 4 only begins on 1 November, the model requires time to detect the forced signal. For the DJF forecasts, the model only has the 30 day transition period from unforced to forced during November to learn the forcing effect. The forecast mean achieves a correlation of 0.48 with the observations of the Dec-Jan-Feb winter mean, despite the limited time to learn the forcing effect. The statistical model notably fails to predict the extreme winter of 2009–10. However, in Figure 7(d) we see that the NAO index did not become unusually negative until mid-December, there was no signal for the model to identify in November.

It would be a mistake to regard the seasonal forecasts from the statistical model as simple

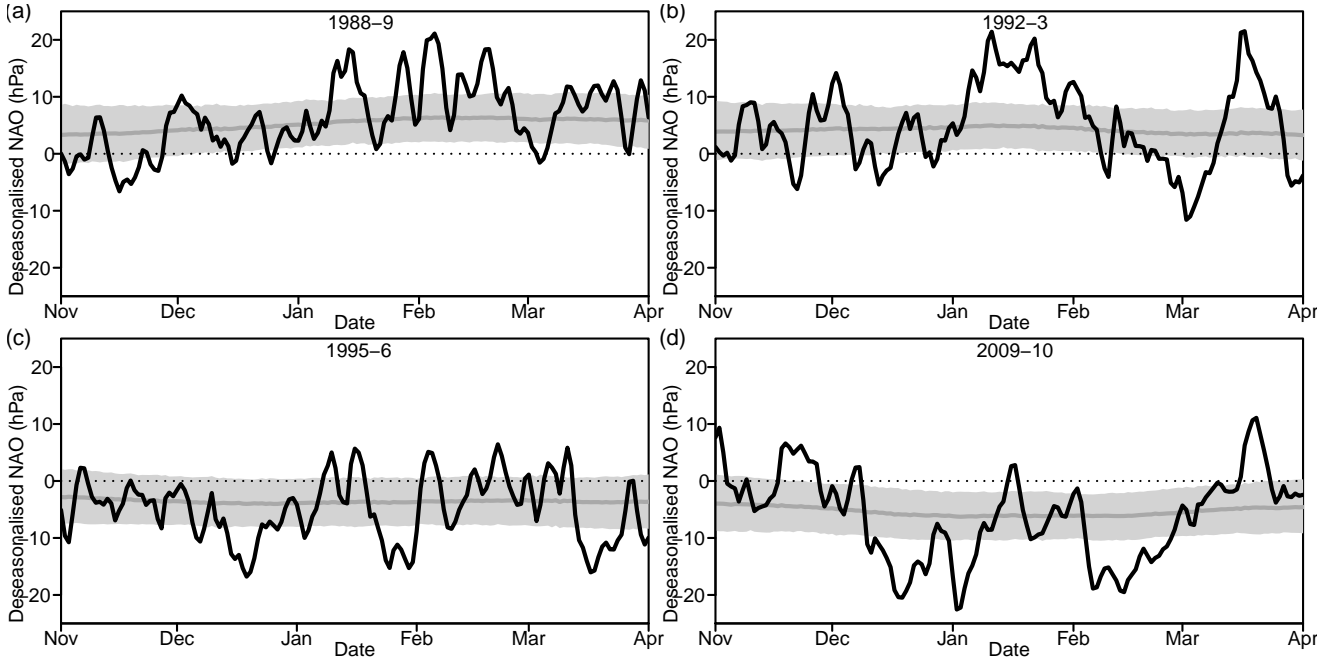


Figure 7: The evolution of the forcing effect δ_t during the winters of 1988–89, 1992–93, 1995–96 and 2009–10. Solid gray lines indicate the mean of 1000 plausible trajectories for the forcing effect δ_t . Shaded regions indicate 95% credible intervals for δ_t computed from the same samples. Solid black lines are the deseasonalized observations for comparison.

persistence forecasts. Extraction of the predictable signal depends on the day-to-day variation in the observed index, not simply the mean of the index in recent observations. For comparison, optimal linearly and exponentially weighted persistence forecasts were computed for the DJF mean NAO index over the same period (see supplementary material for details). The correlations between observations and the exponentially and linearly weighted forecasts are 0.35 and 0.37 respectively. The statistical model outperforms both persistence forecasts.

The forcing effect δ_t does not act on the NAO at all during summer (JJA), and only weakly during the final month of autumn (SON). The weak positive correlation between the forecasts and observations in JJA and SON is due to the long-term trend in Figure 5(a), which is clearly visible in both the forecasts and observations in Figure 8. Since the external forcing appears to influence the NAO index during March and April, we might also expect to have useful predictability for the spring season (MAM). The MAM forecasts in Figure 8 achieve a correlation with the observations of 0.57, making them more skillful than the statistical forecasts for Dec-Jan-Feb. This may appear to contradict the analysis of variance in Table 1 which indicated that a greater proportion of the inter-annual variance was explained by external forcing in winter than in spring. However, by the end of February the model has assimilated three months of additional data with which to estimate the forcing effect. Therefore, the estimate of the forced component is more precise and the forecast becomes more accurate. Jia et al. [2017] and Saito et al. [2017] also found increased skill for MAM forecasts compared to DJF or JFM forecasts.

Weisheimer et al. [2017] noted increased correlation between forecasts of the NAO and observations between 1970–2000 compared to 1950–70. Figure 9 shows correlations for 30-year windows centered on 1970–2001 based on the statistical forecasts in Figure 8. The statistical forecasts show a similar pattern of increasing correlation to that of Weisheimer et al. [2017, Figure 2a]. The pattern of changing skill correlates well with changes in the inter-annual standard deviation of the seasonal mean of the forcing effect δ , also shown in Figure 9. This relationship makes physical sense since if the apparent variability of the forcing effect increases, then so will the signal-to-noise ratio of the predictable signal. However, as in Weisheimer

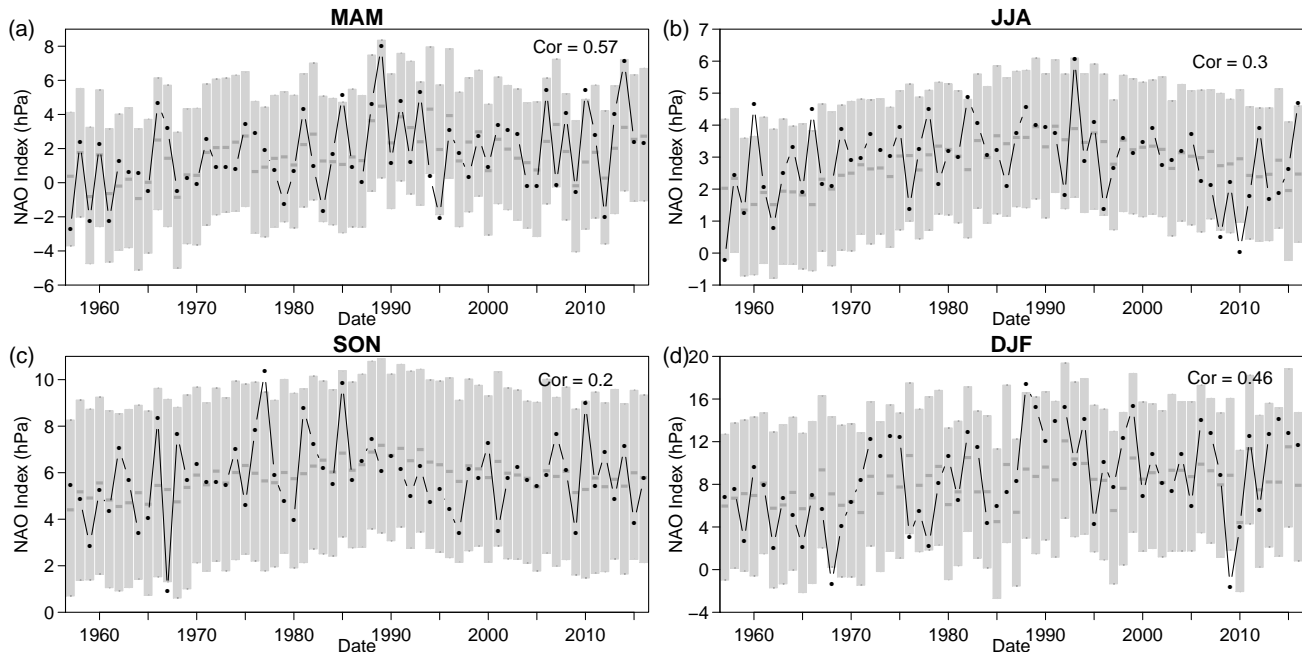


Figure 8: Seasonal forecasting. 1000 forecast members were initialized on 1 March (MAM), 1 June (JJA), 1 September (SON) and 1 December (DJF) every year between 1957 and 2016 and run forwards for three months. Dark gray points indicate the seasonal forecast means. Light gray shaded regions represent the 95% prediction intervals. The observed seasonal mean of the NAO index is plotted in black for comparison.

et al. [2017], we note that the difference in skill between the early 1970s and mid 1990s is not significant.

Figure 10 compares the seasonal forecasts for the winter season (Dec-Jan-Feb) with the state-of-the-art GloSea5 seasonal prediction system for the years 1992–2011. To facilitate the comparison, the ensemble means of both sets of forecasts were recalibrated using linear regression to be compatible with the verifying observations. The statistical forecasts achieve a correlation of 0.53 with the verifying observations, compared to 0.62 for GloSea5. The GloSea5 forecasts are initialized one month earlier, but have the advantage of assimilating data from the entire climate system. In contrast, the statistical model must learn the forcing effect based on only 30 days of NAO index observations. Figure 10 also illustrates a combined forecast using both the GloSea5 and statistical forecasts computed by multiple linear regression of the ensemble means on the observations. The correlation of the combined forecasts with the observations increases to 0.68, suggesting the potential to cheaply update and improve dynamical forecasts with new data using statistical forecasts.

6 Discussion

In this study, we applied state-space modeling techniques to assess persistence and predictability in climate indices. Externally forced predictable signals can be separated from slow changes in the mean and rapid changes due to day-to-day weather. Time series can be analyzed without splitting into seasons since non-stationary mean and seasonal components are estimated at the same time as the predictable signal. We also consider changes in the temporal dependence structure of the index. Our methodology can distinguish predictability due to temporary changes in the mean of an index, from temporary changes in the day-to-day persistence of an index. If the timing of the predictable signal is not known, it can be extracted from the data

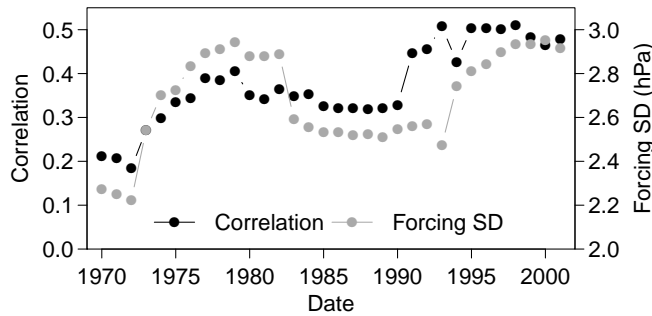


Figure 9: Variation in forecast skill. Correlation between forecasts and observations of DJF mean NAO index, computed for 30-year moving windows between 1956 and 2016. Values are plotted at the 15th year of each window. The inter-annual standard deviation of the DJF mean estimates of the forcing effect δ from Figure 6 are plotted for the same 30-year windows for comparison.

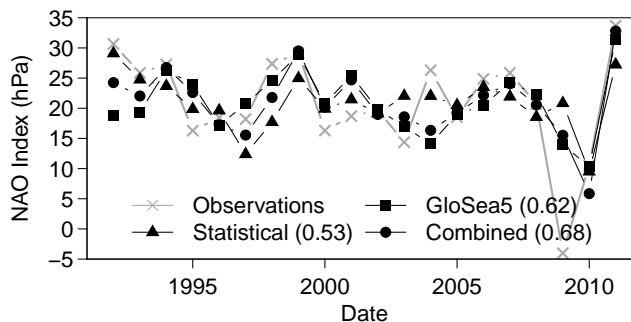


Figure 10: Comparison with GloSea5. Ensemble mean forecasts for DJF each year between 1992 and 2011 from the statistical model and GloSea5. Both sets of forecasts have been recalibrated by linear regression to make them comparable. The GloSea5 verifying observations are plotted for comparison. A combined forecast produced by multiple linear regression of the two sets of ensemble means on the observations is also plotted.

using simple model comparison methods. The individual components of the model have clear physical interpretations, e.g., annual mean, long-term trend, annual cycle, semi-annual cycle etc. This makes it easy to incorporate physical knowledge and intuition through choices in the model structure (e.g., number of harmonic components), initial guesses for component values, and the choices for the model variances.

Existing methods for assessing potential predictability in climate indices only estimate the fractions of inter-annual variance explained by a potentially predictable signal and accumulated weather noise. The methodology demonstrated here provides a wealth of additional information. The variance explained by observation errors and changes in the mean and annual cycle can also be quantified. The state of each component is estimated at every time point, including corresponding uncertainty estimates. Therefore, we can estimate how each component has evolved over the study period. The contribution of each component to individual seasonal means can be also estimated, in addition to the overall variance explained. The predictable signal is treated as a dynamic process, rather than fixed throughout a season, allowing us to estimate changes in the forced signal during a particular season. The same model can also be used for forecasting and can be tested without the need for cross validation.

Our analysis of the daily NAO index suggests a distinct split in the dynamics of the NAO between December, January, February, March and the rest of the year. Focusing on the traditional DJF period, around 60% of the inter-annual variance in the winter mean NAO is attributable

to external forcing, 32% to weather noise and 8% to long-term trends. Our estimate of the contribution of external forcing is similar to that of Franzke and Woollings [2011], but lower than that of Keeley et al. [2009], in part due to the separation of long-term trends from the forced signal. Skillful statistical forecasts of the DJF mean NAO are possible from the end of November and achieve a correlation with the observations of 0.48. Our analysis indicates that external forcing, and hence predictability, extend into March. We found little evidence of potentially predictable signals outside of the extended winter season, although a weak signal may exist for part of boreal summer.

It is striking that the statistical forecast model is able to reproduce the apparent time-varying forecast skill in the NAO noted by Weisheimer et al. [2017]. Dynamical models might be affected by more limited observations of the ocean state in the middle compared to the end of the century, leading to less precise initialization and less skillful forecasts. The statistical model only assimilates observations of the NAO itself, which is likely to be less strongly affected by changes in the observation network, due to the large area the index is averaged over. This suggests that the time-varying predictability may be a physical property of the system. It is also interesting that the statistical model is able to approach the skill of state-of-the-art seasonal forecasting model, although with the caveat of a shorter lead time. Our results suggest possibilities for updating expensive dynamical seasonal forecasts using inexpensive statistical forecasts. Such a hybrid approach might be used to further increase skill through dynamic ensemble design, with additional ensemble members being commissioned dependent on the conditions indicated by the statistical forecasts.

There is a continuing debate over the signal-to-noise ratio of the NAO in dynamical forecast models and its effect on achievable forecast skill [Eade et al., 2014, Shi et al., 2015]. One of the strengths of the methodology described here is its ability to break down time series of climate indices into easily interpretable components. Fitting the statistical model proposed here to long running simulations from dynamical models would enable detailed comparisons between the dynamics of the models and the Earth system. Such detailed benchmarking might lead to new insights into the performance of dynamical models suggest areas for further development. With additional development it may be possible to apply a similar analysis to forecast or hindcast datasets for a more direct comparison.

Acknowledgments

The authors gratefully acknowledge the support of the Natural Environment Research Council grant NE/M006123/1, and Adam Scaife of the UK Met Office for providing the GloSea5 hindcast dataset and for helpful comments on an earlier version of this manuscript.

References

- P. J. Athanasiadis, A. Bellucci, A. A. Scaife, L. Hermanson, S. Materia, A. Sanna, A. Borrelli, C. MacLachlan, and S. Gualdi. A multisystem view of wintertime NAO seasonal predictions. *Journal of Climate*, 30(4):1461–1475, 2017. doi: 10.1175/JCLI-D-16-0153.1.
- M. A. Bourassa, S. T. Gille, C. Bitz, D. Carlson, I. Cerovecki, C. A. Clayson, M. F. Cronin, W. M. Drennan, C. W. Fairall, R. N. Hoffman, G. Magnusdottir, R. T. Pinker, I. A. Renfrew, M. C. Serreze, K. Speer, L. D. Talley, and G. A. Wick. High-latitude ocean and sea ice surface fluxes: Challenges for climate research. *Bulletin of the American Meteorological Society*, 94(3):403–423, 2013. doi: 10.1175/BAMS-D-11-00244.1.
- S. Brönnimann. Impact of El Niño-Southern Oscillation on European climate. *Reviews of Geophysics*, 45(3):RG3003, 2007. doi: 10.1029/2006RG000199.1.INTRODUCTION.
- S. Brönnimann, M. Schraner, B. Müller, A. Fischer, D. Brunner, E. Rozanov, and T. Egorova.

- The 1986-1989 ENSO cycle in a chemical climate model. *Atmospheric Chemistry and Physics*, 6(12):4669–4685, 2006. doi: 10.5194/acp-6-4669-2006.
- F. S. Chapin III, M. Sturm, M. C. Serreze, J. P. McFadden, J. R. Key, A. H. Lloyd, A. D. McGuire, T. S. Rupp, A. H. Lynch, J. P. Schimel, J. Beringer, W. L. Chapman, H. E. Epstein, E. S. Euskirchen, L. D. Hinzman, G. Jia, C.-L. Ping, K. D. Tape, C. D. C. Thompson, D. A. Walker, and J. M. Welker. Role of Land-Surface Changes in Arctic Summer Warming. *Science*, 657(2005):9–13, 2010. doi: 10.1126/science.1117368.
- J. Durbin and S. J. Koopman. *Time Series Analysis by State Space Methods*. Oxford University Press, 2nd edition, 2012. ISBN 9780199641178.
- R. Eade, D. Smith, A. Scaife, E. Wallace, N. Dunstone, L. Hermanson, and N. Robinson. Do seasonal-to-decadal climate predictions underestimate the predictability of the real world? *Geophysical Research Letters*, 41:5620–5628, 2014. doi: 10.1002/2014GL061146.
- D. R. Fereday, A. Maidens, A. Arribas, A. A. Scaife, and J. R. Knight. Seasonal forecasts of northern hemisphere winter 2009/10. *Environmental Research Letters*, 7(3), 2012. doi: 10.1088/1748-9326/7/3/034031.
- C. Franzke and T. Woollings. On the persistence and predictability properties of north atlantic climate variability. *Journal of Climate*, 24(2):466–472, 2011. doi: 10.1175/2010JCLI3739.1.
- L. Jia, X. Yang, G. Vecchi, R. Gudgel, T. Delworth, S. Fueglistaler, P. Lin, A. A. Scaife, S. Underwood, and S. J. Lin. Seasonal prediction skill of northern extratropical surface temperature driven by the stratosphere. *Journal of Climate*, 30(12):4463–4475, 2017. doi: 10.1175/JCLI-D-16-0475.1.
- E. Kalnay, M. Kanamitsu, R. Kistler, W. Collins, D. Deaven, L. Gandin, M. Iredell, S. Saha, G. White, J. Woollen, Y. Zhu, M. Chelliah, W. Ebisuzaki, W. Higgins, J. Janowiak, K. C. Mo, C. Ropelewski, J. Wang, A. Leetmaa, R. W. Reynolds, R. Jenne, and D. Joseph. The NCEP/NCAR 40-year reanalysis project. *Bulletin of the American Meteorological Society*, 77(3):437–471, 1996. doi: 10.1175/1520-0477(1996)077<0437:TNYRP>2.0.CO;2.
- S. P. E. Keeley, R. T. Sutton, and L. C. Shaffrey. Does the North Atlantic Oscillation show unusual persistence on intraseasonal timescales? *Geophysical Research Letters*, 36(22):L22706, 2009. doi: 10.1029/2009GL040367.
- J. Kidston, A. A. Scaife, S. C. Hardiman, D. M. Mitchell, N. Butchart, M. P. Baldwin, and L. J. Gray. Stratospheric influence on tropospheric jet streams, storm tracks and surface weather. *Nature Geoscience*, 8(6):433–440, 2015. doi: 10.1038/NGEO2424.
- C. MacLachlan, A. Arribas, K. A. Peterson, A. Maidens, D. Fereday, A. A. Scaife, M. Gordon, M. Vellinga, A. Williams, R. E. Comer, J. Camp, P. Xavier, and G. Madec. Global Seasonal forecast system version 5 (GloSea5): A high-resolution seasonal forecast system. *Quarterly Journal of the Royal Meteorological Society*, 141(689):1072–1084, 2015. doi: 10.1002/qj.2396.
- R. A. Madden. Estimates of the Natural Variability of Time-Averaged Sea-Level Pressure. *Monthly Weather Review*, 104(7):942–952, 1976. doi: 10.1175/1520-0493(1976)104<0942:EOTNVO>2.0.CO;2.
- R. Prado and M. West. *Time Series: Modelling, Computation and Inference*. Chapman and Hall/CRC, 2010. ISBN 9781420093360.
- N. Saito, S. Maeda, T. Nakaegawa, Y. Takaya, Y. Imada, and C. Matsukawa. Seasonal Predictability of the North Atlantic Oscillation and Zonal Mean Fields Associated with Stratospheric Influence in JMA/MRI-CPS2. *SOLA*, 13:209–213, 2017. doi: 10.2151/sola.2017-038.

- P. G. Sansom, D. B. Williamson, and D. B. Stephenson. State space models for non-stationary intermittently coupled systems. *Journal of the Royal Statistical Society: Series C (Applied Statistics)*, page In review, 2018.
- A. A. Scaife, A. Arribas, E. Blockey, A. Brookshaw, R. T. Clark, N. J. Dunstone, R. Eade, D. Fereday, C. K. Folland, M. Gordon, L. Hermanson, J. R. Knight, D. J. Lea, C. MacLachlan, A. Maidens, M. Martin, K. A. Peterson, D. M. Smith, M. Vellinga, E. Wallace, J. Waters, and A. Williams. Skillful long range prediction of European and North American winters. *Geophysical Research Letters*, 5:2514–2519, 2014. doi: 10.1002/2014GL059637. Received.
- A. A. Scaife, A. Y. Karpechko, M. P. Baldwin, A. Brookshaw, A. H. Butler, R. Eade, M. Gordon, C. MacLachlan, N. Martin, N. Dunstone, and D. Smith. Seasonal winter forecasts and the stratosphere. *Atmospheric Science Letters*, 17(1):51–56, 2016. doi: 10.1002/asl.598.
- W. Shi, N. Schaller, D. Macleod, T. N. Palmer, and A. Weisheimer. Impact of hindcast length on estimates of seasonal climate predictability. *Geophysical Research Letters*, 42(5):1554–1559, 2015. doi: 10.1002/2014GL062829.
- M. Sigmond, J. F. Scinocca, V. V. Kharin, and T. G. Shepherd. Enhanced seasonal forecast skill following stratospheric sudden warmings. *Nature Geoscience*, 6(2):98–102, 2013. doi: 10.1038/ngeo1698.
- D. B. Stephenson, V. Pavan, M. Collins, M. M. Junge, and R. Quadrelli. North Atlantic Oscillation response to transient greenhouse gas forcing and the impact on European winter climate: A CMIP2 multi-model assessment. *Climate Dynamics*, 27(4):401–420, 2006. doi: 10.1007/s00382-006-0140-x.
- L. Tomassini, E. P. Gerber, M. P. Baldwin, F. Bunzel, and M. Giorgetta. The role of stratosphere-troposphere coupling in the occurrence of extreme winter cold spells over northern Europe. *Journal of Advances in Modeling Earth Systems*, 4(10):1–14, 2012. doi: 10.1029/2012MS000177.
- T. Toniazzo and A. A. Scaife. The influence of ENSO on winter North Atlantic climate. *Geophysical Research Letters*, 33(24):1–5, 2006. doi: 10.1029/2006GL027881.
- H. von Storch and F. W. Zwiers. *Statistical Analysis in Climate Research*. Cambridge University Press, 1999. ISBN 0521450713.
- A. Weisheimer, N. Schaller, C. O’Reilly, D. A. MacLeod, and T. Palmer. Atmospheric seasonal forecasts of the twentieth century: multi-decadal variability in predictive skill of the winter North Atlantic Oscillation (NAO) and their potential value for extreme event attribution. *Quarterly Journal of the Royal Meteorological Society*, 143(703):917–926, 2017. ISSN 1477870X. doi: 10.1002/qj.2976.
- D. Wilks. *Statistical Methods in the Atmospheric Sciences*. Academic Press, third edition, 2011. ISBN 9780123850225.
- F. W. Zwiers. A Potential Predictability Study Conducted with an Atmospheric General Circulation Model. *Monthly Weather Review*, 115(12):2957–2974, 1987. doi: 10.1175/1520-0493(1987)115<2957:APPSCW>2.0.CO;2.

State-space modeling of intra-seasonal persistence in daily climate indices: a data-driven approach for seasonal forecasting

Philip G. Sansom, David B. Stephenson and Daniel B. Williamson
University of Exeter, Exeter, United Kingdom

Supplementary material

1 Exploratory analysis

The aim of the exploratory analysis is to identify the number of harmonic components K required to represent any annual cycle in the observations, the order P of the autoregressive process required to represent the weather, and any other features that may need to be included in the model. The periodogram in Figure 1(a) suggests that the NAO index contains annual and semi-annual cycles, i.e., $K = 2$.

The observed index was linearly detrended and fixed annual and semi-annual cycles removed by linear regression before examining the autocorrelation structure. The autocorrelation and partial autocorrelation functions in Figures 1(c) and (d) both decay rapidly, indicating that an autoregressive process is a good representation of the day-to-day variability. The partial autocorrelation function is approximately zero at lags greater than five, suggesting an AR(5) process for the weather variability, i.e., $P = 5$.

Figure 1(b) shows the inter-annual variance in the first differences (e.g., $y_t - y_{t-1}$) of the NAO index computed for each day of the year. There is a clear annual cycle in the day-to-day variability of the NAO index. The day-to-day variability is represented in our model by the variance W_X . We model the annual cycle in the day-to-day variance as

$$W_{Xt} = W_X + \sqrt{a^2 + b^2} + a \sin \omega t + b \cos \omega t \quad W_X > 0.$$

The parameters W_X , a and b are assumed to be constant and are estimated by maximum likelihood with the other variance parameters.

2 Initial guesses for state variables

Our initial guesses for the state variables $\mu_t, \beta_t, \psi_{1t}, \psi_{1t}^*, \dots, \psi_{Kt}, \psi_{Kt}^*, X_t, \dots, X_{t-P+1}, \phi_{1t}, \dots, \phi_{Pt}$ at time $t = 0$ are shown in Table 1. The initial guess for μ_t at $t = 0$ is based on Figure 7 of Hsu and Wallace [1976] which suggests an overall mean of 4 hPa–8 hPa. The prior on the local trend β_t is based on our judgment that the NAO mean is unlikely experience a local change equivalent to more than 1 hPa/yr. The analysis of Chen et al. [2012] suggests an annual cycle of approximately 4 hPa and a semi-annual cycle of around 2 hPa. The daily NAO index in Figure 1(a) of the main study has a range of approximately 40 hPa. Therefore, the TVAR residuals X_0, \dots, X_{1-p} were assigned independent normal priors mean 0 hPa and variance 10^2 . Masala [2015] fitted an AR(5) model to NAO data and found coefficients of alternating sign in the range (-1.3,+1.8). Therefore,

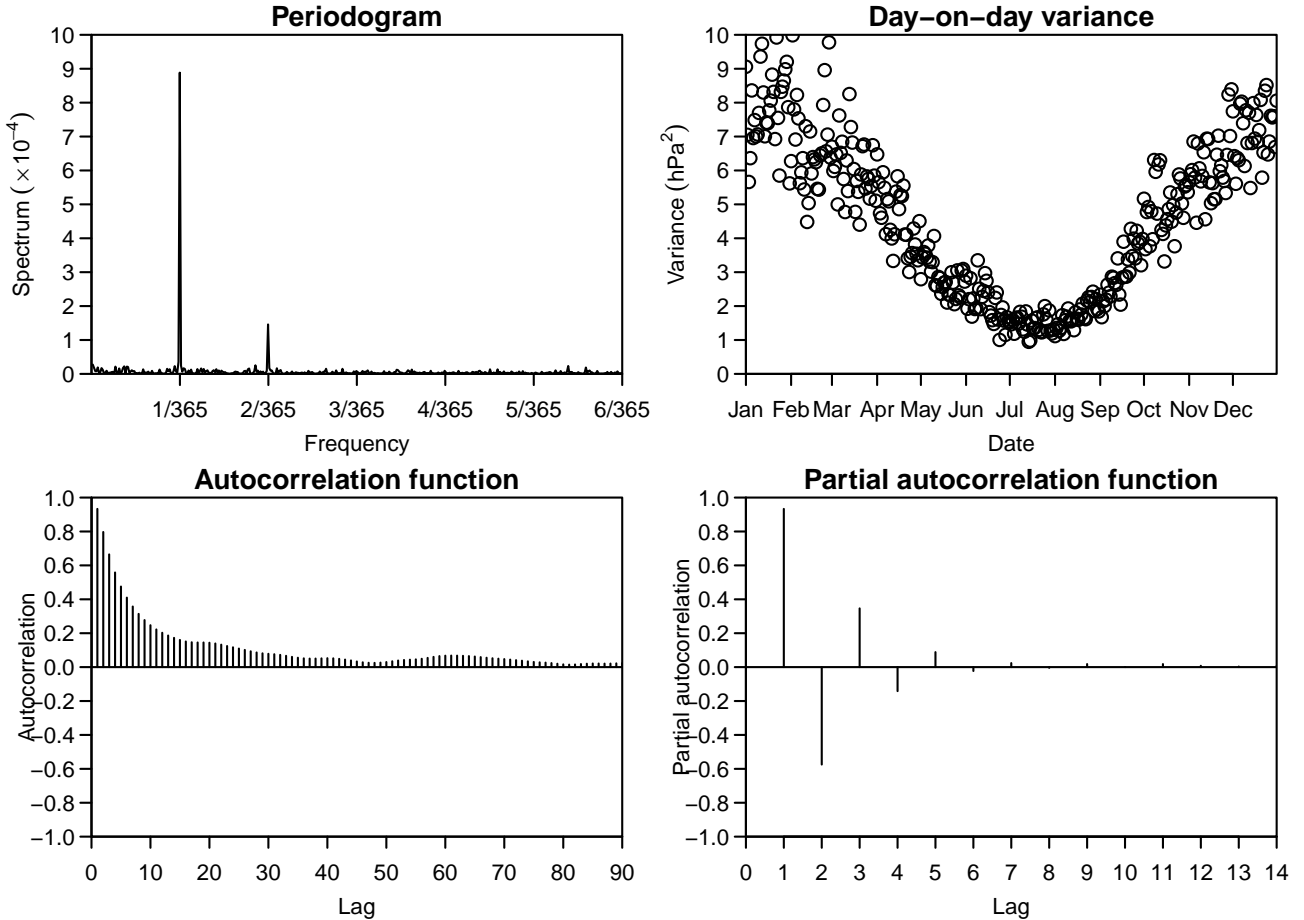


Figure 1: Exploratory analysis. (a) Periodogram, (b) day-on-day variance of first differences, (c) autocorrelation function, and (d) partial autocorrelation function of the daily NAO index.

the TVAR coefficients $\phi_{10}, \dots, \phi_{p0}$ were assigned independent normal priors with means given by the estimates of Masala [2015] and variance 0.2^2 .

The inter-annual standard deviation of the winter mean NAO index is approximately 5 hPa according to Figure 1 of the main study. Therefore, our initial guess for the forcing effect δ_t at $t = 0$ in the mean effect model is 0 hPa, with variance 5^2 . The change in the autoregressive coefficients under the autocorrelation effect model is not expected to be large. Therefore, our initial guess for the forcing effects δ_{pt} at time $t = 0$ in the autocorrelation model has mean 0 and variance 0.2^2 .

3 Estimation of the variance parameters

The variance parameters $V, W_\mu, W_\beta, W_\psi, \sigma_X^2, a_X, b_X, W_\phi, W_\delta$ and the coefficient φ must be estimated in order to fit the model. The model fitting procedures developed by Sansom et al. [2018] include efficient calculation of the likelihood. Therefore, the unknown parameters can be easily estimated by maximum likelihood. Numerical optimization of the likelihood was performed using the Broyden-Fletcher-Goldfarb-Shanno algorithm as implemented in the R programming language. For parsimony, the variances W_μ and W_ψ were assumed to be equal since. In order to enforce the constraint that the variance parameters are all positive, optimization was performed

Component	Parameter	Mean	Variance
Mean	μ	6 hPa	2^2
Local trend	β	0 hPa/yr	0.002^2
Annual cycle	ψ_1, ψ_1^*	0 hPa	3^2
Semi-annual cycle	ψ_2, ψ_2^*	0 hPa	2^2
Weather noise	X_t, \dots, X_{t-p+1}	0 hPa	10^2
AR coefficients	ϕ_1, \dots, ϕ_p	0	1^2

Table 1: Initial guesses for the state variables. The initial guesses are normally distributed and express our prior uncertainty about the value of the state variables at time $t = 0$.

Component	Parameter	Estimate
Long-term mean	W_μ	3.5×10^{-8}
Local trend	W_β	2.8×10^{-12}
Forcing coefficient	φ	0.995
Forcing variance	W_δ	1.3×10^{-1}
AR coefficients	W_ϕ	6.1×10^{-12}
Weather noise	W_X	2.39
	a_X	0.39
	b_X	1.64
Observation error	V	2.5×10^{-5}

Table 2: Maximum likelihood estimates of the model parameters.

on the log scale for V , W_μ , W_β , W_X , W_ϕ , W_δ . The coefficient φ is expected to lie in the range $(0, 1)$ so was fitted on a logistic scale. The maximum likelihood estimates of the parameters for the final model with $K = 2$ and $P = 6$ are shown in Table 2

4 Posterior predictive checks

Figure 2 shows the results of the posterior predictive checks on the initial model with $K = 2$, $P = 5$ and 180 day forced period (Nov-Dec-Jan-Feb-Mar-Apr). Posterior predictive simulations were started from 1968 to give the model time to learn the systematic components (mean, annual cycle, TVAR coefficients). The model appears to capture the inter-annual variance in Figure 2(a). Figure 1(c) of the main text showed a distinct difference in the autocorrelation structure between Dec-Mar and Apr-Nov, therefore we focus on the autocorrelation functions of these two periods. Figure 2(b) shows that the model with $P = 5$ is unable to reproduce the observed autocorrelation structure during Apr-Nov. The simulated autocorrelation is more like that of Dec-Mar. Examining the autocorrelation functions by month revealed that the shift was due to the simulated autocorrelation during April being more like Dec-Mar than May-Nov. This suggests that the length of the forced is too long. Figure 3 shows that reducing the end of the forced period by two weeks to mid-March increases the separation between the simulated autocorrelation functions and improves the simulation of the inter-annual variance. However, the model is still unable to properly capture the autocorrelation structure in Apr-Nov. Fitting additional models with autoregressive components of varying order ($P = 3, 4, 5, 6, 7$) revealed that the model with $P = 6$ is able to capture the observed autocorrelation structure.

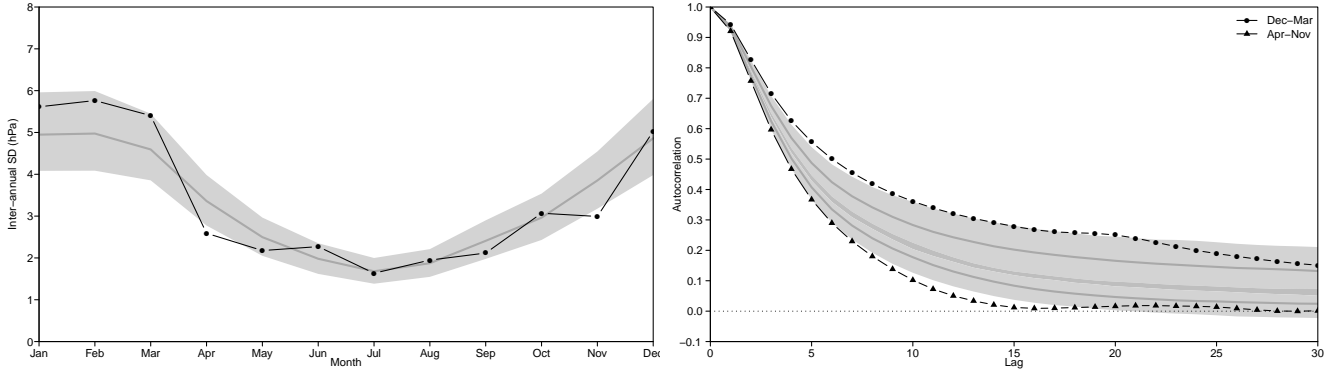


Figure 2: Posterior predictive checks. (a) The inter-annual standard deviation of the monthly mean NAO index, and (b) the autocorrelation function of the daily NAO index computed for Dec-Mar and Apr-Nov. Black lines represent the sample estimates computed from the observed NAO index as in Figure 1 of the main text. Shaded grey regions represent 95% credible intervals computed from 1000 simulations of the 50 years between 1968 and 2017 from the statistical model.

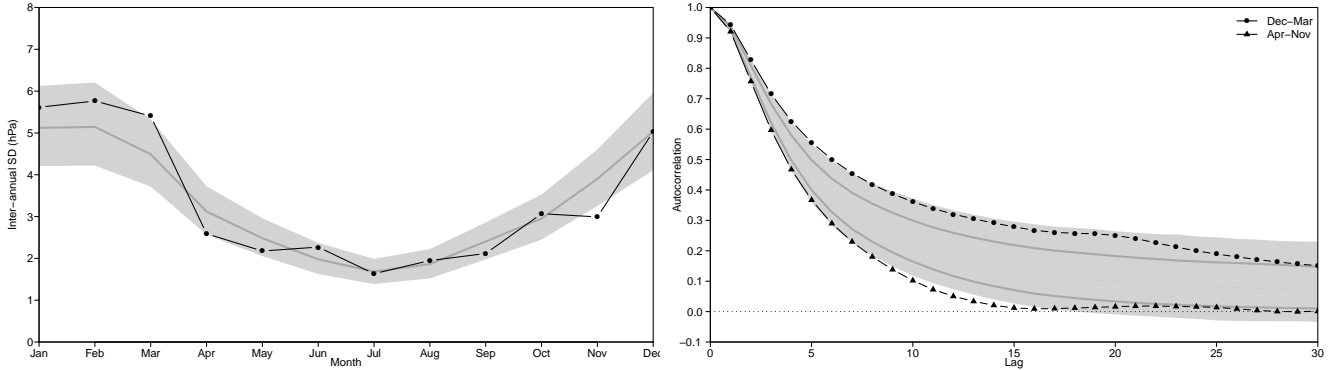


Figure 3: As in Figure 2 but for the model with coupled period reduced by two weeks.

5 Persistence forecasts

The linearly weighted persistence forecast \hat{Y}_L at time t is defined as the mean of the previous K observations

$$\hat{Y}_{Lt} = \frac{1}{K} \sum_{k=1}^K Y_{t-k}$$

the optimal value of K was selected as the value that maximized the correlation between the observed winter (DJF) means and the forecasts in Figure 4(a).

The exponentially weighted persistence forecast \hat{Y}_E at time t is defined by the recursion

$$\begin{aligned} \hat{Y}_{E1} &= Y_1 \\ \hat{Y}_{Et} &= \alpha Y_t + (1 - \alpha) \hat{Y}_{E,t-1} \quad t > 1 \end{aligned}$$

the optimal value of α was selected as the value that maximized the correlation between the observed winter (DJF) means and the forecasts in Figure 4(b).

It should be noted that the correlations achieved by the persistence forecasts are probably over-estimates, since no cross-validation design was used.

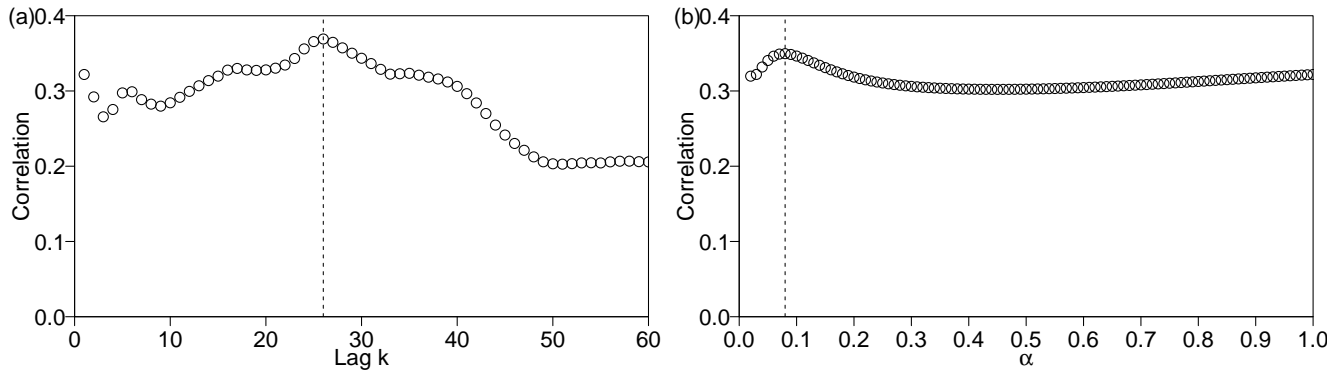


Figure 4: Optimal persistence forecasts. Comparison of (a) different lags k for the linearly weighted forecast, and (b) different parameters α for the exponentially weighted forecast. The mean, annual cycle and semi-annual cycle were estimated by least squares and removed from the observations before fitting.

References

- G. Chen, C. Qian, and C. Zhang. New Insights into Annual and Semiannual Cycles of Sea Level Pressure. *Monthly Weather Review*, 140(4):1347–1355, 2012. doi: 10.1175/MWR-D-11-00187.1.
- C.-P. F. Hsu and J. M. Wallace. The Global Distribution of the Annual and Semiannual Cycles in Sea Level Pressure. *Monthly Weather Review*, 104(12):1597–1601, 1976. doi: 10.1175/1520-0493(1976)104<1597:TGDOTA>2.0.CO;2.
- G. Masala. North Atlantic Oscillation index stochastic modelling. *International Journal of Climatology*, 35:3624–3632, 2015. doi: 10.1002/joc.4236.
- P. G. Sansom, D. B. Williamson, and D. B. Stephenson. State space models for non-stationary intermittently coupled systems. *Journal of the Royal Statistical Society: Series C (Applied Statistics)*, page In review, 2018.